PHYSICS

Time-independent harmonics dispersion relation for time-evolving nonlinear waves

Romik Khajehtourian[1]† and Mahmoud I. Hussein[2,3]*†

We present a theory for the dispersion of generated harmonics in a traveling nonlinear wave. The harmonics dispersion relation (HDR), derived by the theory, provides direct and exact prediction of the collective harmonics spectrum in the frequency–wave number domain and does so without prior knowledge of the $u = u(x, t)$ solution. It is valid throughout the evolution of a distorting unbalanced wave or the steady-steady propagation of a balanced wave with waveform invariance. The new relation is shown to be a special case of the general nonlinear dispersion relation (NDR), which is also derived. The theory is examined on a diverse range of cases of one-dimensional elastic waves and shown to hold irrespective of the spatial form of the initial wave profile, type and strength of the nonlinearity, and the level of dispersion in the linear limit. Another direct outcome of the general NDR is an analytical condition for soliton synthesis.

INTRODUCTION

Wave motion lies at the heart of many disciplines in the physical sciences and engineering. For example, natural phenomena involving atomic motion, seismic motion, fluid flow, heat transfer, or propagation of light and sound all involve wave physics at some level (*1*). While the theory of linear dispersive waves is fairly complete, much has remained to be understood about nonlinear waves and their characterization. For linear systems, it is customary to obtain dispersion relations that relate the frequency ω and wave number κ of propagating modes. A dispersion relation provides valuable information and is often used to characterize a range of physical properties of the medium admitting the wave motion (*2*). In nonlinear systems, on the other hand, the notion of a dispersion relation has been treated with caution because superposition does not apply. Yet, the appeal of retaining nonlinear effects in the study of dispersion has motivated several studies in a variety of disciplines, including quantum mechanics (*3*), solid mechanics (*4*–*9*), fluid dynamics (*10*–*13*), acoustics (*14*), electromagnetics (*15*, *16*), plasma physics (*17*–*20*), geophysics (*21*–*23*), astrophysics (*24*), and biophysics (*25*, *26*), among others. Aside from explicit examination of dispersion, classical methods for solving the initial-value problem for a wide class of nonlinear evolution equations have been developed since the late 1960s (*27*–*30*).

In many problems, it is often sufficient to consider the effects of weak nonlinearities; in such cases, these effects are augmented over the linear dispersion relation in the form of perturbations (*31*). Nonlinear dispersion relations for systems exhibiting weak nonlinearities were derived by small-parameter expansions, for example, for discrete chains (*5*, *7*), elastic rods (*4*), and plasma (*17*). For strong nonlinearities, however, exact derivations of NDR are needed. While relatively rare, a few exact NDR formulations have been produced for certain problems; for example, Schürmann *et al.* (*32*) provided an exact NDR for TE-polarized electromagnetic waves in a layered structure and Huang *et al.* (*18*) and Ginzburg *et al.* (*19*) for surface plasmon waves.

However, a key question remains, and that is what does it mean to have a dispersion relation for nonlinear waves, especially when the nonlinearity is strong? One challenge stems from the fact that an unbalanced nonlinear wave distorts as it travels and appears to ultimately fully lose its original shape, and in many instances, the final outcome is onset of a form of instability (*1*). Inherent to this distortion is an intricate mechanism of harmonic generation, a phenomenon that is widely used in laser science (*33*) and ultrasound nondestructive evaluation (*34*–*36*). Harmonic generation also takes place in balanced waves that do not experience distortion (*37*). In the presence of harmonic generation, a Fourier transform of the space-time response reveals a fundamental harmonic and a series of higher-order harmonics. The distortion that we observe is a manifestation of energy exchange from one harmonic to the other (*38*, *39*). Aside from dispersion analysis, rigorous theory has been developed for the analysis of the spatial response of multiple harmonics. Early works in this area include papers by Thurston and Shapiro (*40*), Tiersten and Baumhauer (*41*), and Thompson and Tiersten (*42*). Common techniques applied on weakly nonlinear systems seek spatial solutions for harmonics using perturbation expansions, e.g., see publications on elastic waves by Auld (*43*), Deng (*44*), and de Lima and Hamilton (*45*). This body of theory follows key experimental work on harmonic generation in ultrasonic waves in metals (*34*–*36*, *46*, *47*); see review by Matlack *et al.* (*48*).

In an earlier study (*8*), we presented an exact dispersion relation for a thin elastic rod modeled by a nonlinear second-order partial differential equation (PDE). The term "thin" designates a rod model with a cross-sectional thickness much smaller than the wavelengths of the propagating waves; a thin rod is nondispersive in the small-amplitude linear limit. Validation by numerical simulation was performed, whereby a cosine waveform with a specific value of amplitude and a specific value of wave number was initially prescribed and the derived NDR was shown to predict, exactly, the instantaneous change in the frequency from what is otherwise dictated by the linear dispersion relation. No connection was established between the derived NDR and the evolved nonlinear wave, either in its spatial form or by considering its generated harmonics. An elastic

[1]Department of Mechanical and Process Engineering, ETH-Zürich, Zürich 8092, Switzerland. [2]Ann and H.J. Smead Department of Aerospace Engineering Sciences, University of Colorado Boulder, Boulder, CO 80303, USA. [3]Department of Physics, University of Colorado Boulder, Boulder, CO 80302, USA.
*Corresponding author. Email: mih@colorado.edu
†These authors contributed equally to this work.

beam, modeled by a fourth-order PDE, was also investigated by the same approach, and an exact NDR was derived for a simplified version of that system (*49*); however, no validation by numerical simulation was performed, as the model appeared overly complex to integrate numerically.

Here, we provide a theory that characterizes the nature of a nonlinear wave, through its harmonic generation, as it evolves over long times. The prediction is in the form of an exact analytical dispersion relation that describes the distribution of the generated harmonics in the frequency–wave number domain; it is valid at all times for a balanced wave or up to the point of breaking if the wave reaches an unstable state. This result thus introduces a new insight into the notion of an NDR and a new finding pertaining to the spectral characterization of harmonic generation.

We present the theory not only for a thin rod but also for a thick rod. A "thick" rod is modeled by a fourth-order PDE, exhibits lateral inertia, and is dispersive in the linear limit as the wave amplitude $B \to 0$. For both systems, we first derive a general NDR as a function of B and wave number κ and then specialize our derivation to yield a harmonics dispersion relation that predicts the harmonic generation spectrum associated with a wave having an initially prescribed amplitude–wave number pair: $B = B_e$ and $\kappa = \kappa_e$. Upon presenting the theory, we provide validation by numerical simulation followed by Fourier transformation, demonstrating applicability for (i) large amplitudes, (ii) different types of nonlinearity, (iii) different times throughout the evolution, (iv) the presence or lack of dispersion in the linear limit, and (v) different initial wave profiles. Last, we provide an analytical condition for soliton synthesis, which represents yet another outcome of the general NDR.

RESULTS

Theory

Thick elastic rod

We consider an infinite one-dimensional (1D) rod with polar radius of gyration r and constant material properties. The rod admits longitudinal displacements $u(x, t)$ under uniaxial stress $\sigma(x, t)$, where x and t denote position and time, respectively. The governing nonlinear equation of motion (EOM) is obtained by Hamilton's principle $\delta \int_0^t (\mathcal{T} - \mathcal{U})\, \partial t = 0$, where $\mathcal{T} = \rho\,[(\partial_t u)^2 + \nu^2 r^2 (\partial_{tx}^2 u)^2]/2$ and $\mathcal{U} = \sigma\epsilon/2$ define the kinetic and strain energy densities, respectively. Here, ρ and ν denote the mass density and Poisson's ratio, and the stress in our model follows Hook's law $\sigma = E\epsilon$, where E is the elastic modulus. A linear constitutive law is considered for simplicity, but the theory is directly applicable to material nonlinearities as well. Geometric nonlinearity is introduced through the definition of strain; a finite strain ϵ may, in principle, take the form of any of the Seth-Hills family of strain measures (*50*, *51*). Here, we consider, separately, the Green-Lagrange strain (GLS) and Hencky strain (HS) measures, which are defined as $\epsilon = \partial_x u + (\partial_x u)^2/2$ and $\epsilon = \ln(1 + \partial_x u)$, respectively. The EOM for the displacement gradient $\bar{u} = \partial_x u$ takes the general form

$$\partial_{tt}\bar{u} - \partial_{xx}(\alpha\bar{u} + \beta\mathcal{N}(\bar{u}) + \gamma\,\partial_{tt}\bar{u}) = 0 \tag{1}$$

where $\alpha = \beta = c^2$ and $\mathcal{N}(\bar{u}) = 3\bar{u}^2/2 + \bar{u}^3/2$ for the GLS measure and $\alpha = 0$, $\beta = c^2$, and $\mathcal{N}(\bar{u}) = \ln(1 + \bar{u})/(1 + \bar{u})$ for the HS measure. For both cases, the quasistatic speed of sound is given by $c = \sqrt{E/\rho}$, and for compactness, we have introduced the parameter $\gamma = r^2\nu^2$. In this model, the effect of the lateral inertia is considered only on the longitudinal displacement; however, the theoretical framework is fully valid in the absence of this modeling simplification.

For the limiting configuration of a thin rod, the lateral inertia is omitted by setting $r = 0$. In this medium, a traveling wave profile with an initial finite-amplitude B_e will experience, in the course of its evolution, forward self-steepening in the case of Green-Lagrange nonlinearity and backward self-steepening in the case of Hencky nonlinearity. Eventually, each wave experiences instability at time τ_S. An analysis of this steepening effect and its path to instability is given in the Supplementary Materials, where in fig. S1, both self-steepening scenarios are demonstrated.

General nonlinear dispersion relation

We introduce a traveling phase variable $\xi = \kappa x - \omega t$ and substitute it into Eq. 1, resulting in the transformation from $\bar{u}(x, t)$ to $\bar{U}(\xi)$. This gives

$$\omega^2 \bar{U}_{\xi\xi} - \kappa^2(\alpha\bar{U} + \beta\mathcal{N}(\bar{U}) + \omega^2\gamma\,\bar{U}_{\xi\xi})_{\xi\xi} = 0 \tag{2}$$

which, upon integration twice, yields

$$(\kappa^2\alpha - \omega^2)\,\bar{U} + \kappa^2\beta\mathcal{N}(\bar{U}) + \gamma\kappa^2\omega^2\,\bar{U}_{\xi\xi} = 0 \tag{3}$$

The integration constants leading to Eq. 3 represent coefficients of a constant term and a secular term and have been set equal to zero, which is consistent with a bounded traveling wave solution for an initially bounded displacement field.

Now, we seek a general NDR that we associate with any arbitrary initial waveform $\bar{f}(x, 0)$ belonging to the family of wave functions $\mathcal{F}$ that is consistent with the following conditions at $\xi = 0$

$$\bar{U}(0) = B\kappa,\ \bar{U}_\xi(0) = 0,\ \bar{U}_{\xi\xi}(0) = -B\kappa \tag{4}$$

The choice of "$B\kappa$" is not unique, but this quantity is selected because the deviation from the linear dispersion curve depends directly on this product. Setting $\xi = 0$, by definition, restricts the spatial (κx) and temporal (ωt) phases to be equal. This, in turn, enables a moving reference frame that follows the traveling wave, which allows for a time-independent nonlinear dispersion analysis. Examples of $\mathcal{F}$ functions include cosine, hyperbolic secant, Gaussian, and Lorentzian functions. Upon substitution of Eq. 4 into Eq. 3, we obtain the exact NDR for the GLS and HS measures, respectively, as

$$\omega^{\mathrm{GLS}} = c\kappa\sqrt{(2 + 3B\kappa + B^2\kappa^2)/(2 + 2\gamma\kappa^2)} \tag{5}$$

and

$$\omega^{\mathrm{HS}} = c\kappa\sqrt{\ln(1 + B\kappa)/(B\kappa(1 + B\kappa)(1 + \gamma\kappa^2))} \tag{6}$$

These reduce to a linear dispersive form in the limit of $B \to 0$ and a linear nondispersive form in the limit $B \to 0$, $\gamma \to 0$. Figure 1D presents a plot of the general NDR for the GLS model, as defined in Eq. 5, for a thin rod and $B = 0.0125$ (see solid red curve). Note that nonlinearity by itself causes wave dispersion (*8*).

Harmonics dispersion relation

We now uncover that the general NDR derived above inherently encompasses information on the harmonic generation mechanism associated with nonlinear waves characterized initially by a specific

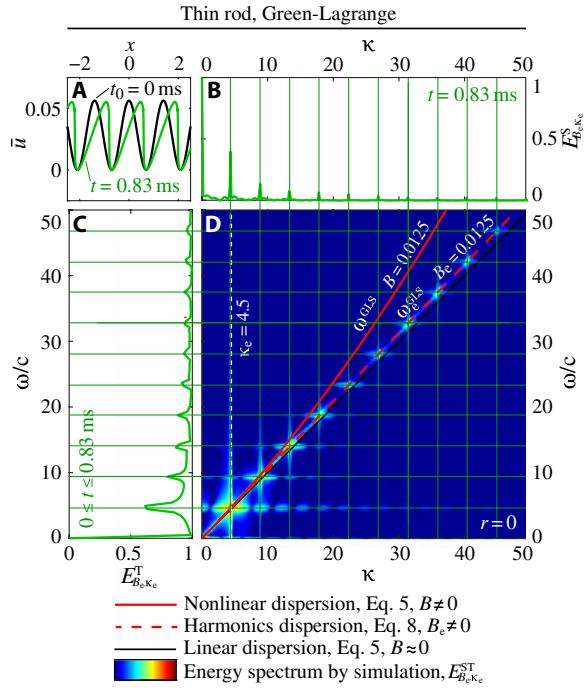

Fig. 1. Nonlinear cosine wave experiencing distortion (steepening) and harmonic generation. (**A**) Spatial profiles captured at the initial time and at a later time; initial amplitude is $B_e = 0.0125$, and initial wave number is $\kappa_e = 4.5$. (**B**) Wave number spectrum, (**C**) frequency spectrum, and (**D**) frequency–wave number spectrum of harmonics demonstrating exact prediction by the harmonics dispersion relation of Eq. 8. The result is based on the GLS measure.

amplitude $B = B_e$ and wave number $\kappa = \kappa_e$. Starting with Eq. 3, we impose the set of conditions

$$\bar{U}(0) = B_e\kappa_e, \bar{U}_\xi(0) = 0, \bar{U}_{\xi\xi}(0) = -B_e\kappa_e \tag{7}$$

which is a special case of the conditions prescribed in Eq. 4. This yields the following exact harmonics dispersion relation for the GLS and HS models, respectively

$$\omega_e^{GLS} = c\kappa\sqrt{(2 + 3B_e\kappa_e + B_e^2\kappa_e^2)/(2 + 2\gamma\kappa^2)} \tag{8}$$

and

$$\omega_e^{HS} = c\kappa\sqrt{\ln(1 + B_e\kappa_e)/(B_e\kappa_e(1 + B_e\kappa_e)(1 + \gamma\kappa^2))} \tag{9}$$

Each of these relations predicts the exact frequency–wave number curve on which all the harmonics will lie following a Fourier transform of the time response of a traveling nonlinear pulse of any arbitrary form provided that the initial conditions of the solved PDE are consistent with the corresponding $\xi = 0$ conditions stated in Eq. 7. If the pulse is not balanced, e.g., is experiencing self-steepening, then the prediction will be valid up to time τ_S, the instant of onset of instability. Alongside the general NDR curve plotted in Fig. 1D for the thin-rod GLS model, a harmonics dispersion relation based on Eq. 8 is plotted for $B_e = 0.0125$ and $\kappa_e = 4.5$ (see dashed red curve). The notion of a harmonics dispersion relation represents a new paradigm in nonlinear wave science.

Single generic forms of the general NDR and the harmonics dispersion relation in terms of the nonlinear function, $\mathcal{N}(\bar{U})$, and the strain gradient at $\xi = 0$, $\bar{U}(0)$, for the two types of nonlinearity, are provided in the Supplementary Materials. These generic forms allow us to apply the general NDR and the harmonics dispersion relation to other types of nonlinearities in a modular fashion.

Validation by direct numerical simulations

In this section, we seek a numerical solution of Eq. 1 to validate our assertion that each of Eqs. 8 and 9 (for the GLS and HS measures, respectively) represents a dispersion relation for harmonic generation. We use a spectral method in conjunction with an efficient explicit time-stepping method to obtain the response as a function of position and time. Afterward, a discrete Fourier transform is performed on the simulated space-time field to reveal the spectrum of the emerging harmonics and compare their distribution in the frequency–wave number domain with the analytically derived harmonics dispersion relation (see the Supplementary Materials for details on the numerical approach).

We consider a 1D computational domain and prescribe initially as an "excitation" a spatially harmonic or a solitary wave profile that is characterized by an amplitude B_e and a wave number κ_e. In principle, any arbitrary but well-defined and smooth wave function $\bar{f}(x,0) \in \mathcal{F}$ that is consistent with Eq. 7, which are the conditions used to derive the harmonics dispersion relation, may be used in these simulations. Once a function $\bar{f}(x,0)$ is selected, we set $\bar{u}(x,0) = B_e\kappa_e[1 + \bar{f}(x,0)/(B_e\kappa_e)]/2$; the "1/2" offset is introduced as a preprocessing step to facilitate direct comparison with theory. The space-time domain is defined by $-x^* < x \le x^*$ (large enough to allow an unbalanced nonlinear wave to fully evolve up to the point of breaking) with a grid spacing of $h = 1$ cm and $0 \le t \le \tau_S$ with a constant time step of $\Delta t = 1$ μs.

First, we examine a simple cosine wave profile [for which $\bar{f}(x,t) = B_e\kappa_e\cos(\kappa_e(x - ct))$] as an excitation signal and apply it to the case of the thin rod with GLS nonlinearity. This wave profile has the form $\bar{u}(x,t) = B_e\kappa_e[1 + \cos(\kappa_e(x - ct))]/2$ and is characterized by $B_e = 0.0125$ and $\kappa_e = 4.5$. We prescribe this $\bar{u}$ field along the entire computational domain at initial time $t = t_0 = 0$ and let the simulation run freely afterward. Periodic boundary conditions are applied for all simulations involving a cosine signal excitation; otherwise, when a localized excitation is prescribed, the simulations are not allowed to run beyond the time when boundary reflections occur. A time snapshot of the simulated motion is plotted in Fig. 1A, showing a clear distortion of the wave profile after some traveling time. This distortion is caused by the nonlinear GLS inherently present in the model.

Performing Fourier analysis separately in space and in time on the evolved wave field, on a time window that ends at $t = 0.83$ ms, indicates the generation of harmonics in both the wave number and frequency domains. The spatial energy spectrum $E^S_{B_e,\kappa_e}$ and the temporal energy spectrum $E^T_{B_e,\kappa_e}$ are plotted in Fig. 1(B and C, respectively) (the subscripts indicate that the spectrum is associated with a prescribed initial wave with amplitude B_e and wave number κ_e). In Fig. 1D, we show the contour of $E^{ST}_{B_e,\kappa_e} = \ln|\mathcal{E}^{ST}_{B_e,\kappa_e}|$, where $\mathcal{E}^{ST}_{B_e,\kappa_e}$ is the evolved energy spectrum produced by Fourier analysis in both space and time, noting that the Fourier transformation is always done at a time close to τ_S (see the Supplementary Materials for details of the numerical scheme). The brightened areas in the contour plot represent the harmonics, which are consistent with each of the separately obtained spatial (Fig. 1B) and temporal (Fig. 1C) harmonics.

The frequency–versus–wave number distribution of the generated harmonics, as produced by standard direct simulations, accurately coincides with the theoretical harmonics dispersion curve derived in Eq. 8, thus providing firm validation of the theory.

Validation for large wave amplitudes and different types of nonlinearity

We repeat the simulation of Fig. 1, considering higher amplitudes and also considering both the GLS and HS models. In Fig. 2A, we show the time evolution of the same cosine wave but for initial amplitudes $B_e = 0.025$, 0.05, and 0.075, and, in Fig. 2B, provide the corresponding energy spectra in the frequency–wave number domain. For all cases, the harmonics dispersion relation of Eq. 8 perfectly predicts the distribution of the harmonics. In Fig. 3, we extend the excitation signal amplitude further to a value of $B_e = 0.1$ and, once again, show perfect prediction. A wave with an initial amplitude of $B_e = 0.1$ is considered strongly nonlinear; this is evident from the significant deviation of the general NDR curve for $B = 0.1$ compared to the infinitesimal dispersion relation. The validation is successful not only for the GLS model (which exhibits a hardening nonlinearity) but also for the HS model (which exhibits a softening nonlinearity), thus demonstrating generality of the theory to different types of nonlinearities.

Validation throughout wave evolution

Now, we consider the validity of the harmonics dispersion relation at different stages of evolution of a nonlinear wave. We refer again to Fig. 3 where, in Fig. 3A, we show the initial cosine signal corresponding to $B_e = 0.1$ and $\kappa_e = 4.5$ and overlay two subsequent time snapshots of the simulated motion. Performing Fourier analysis in

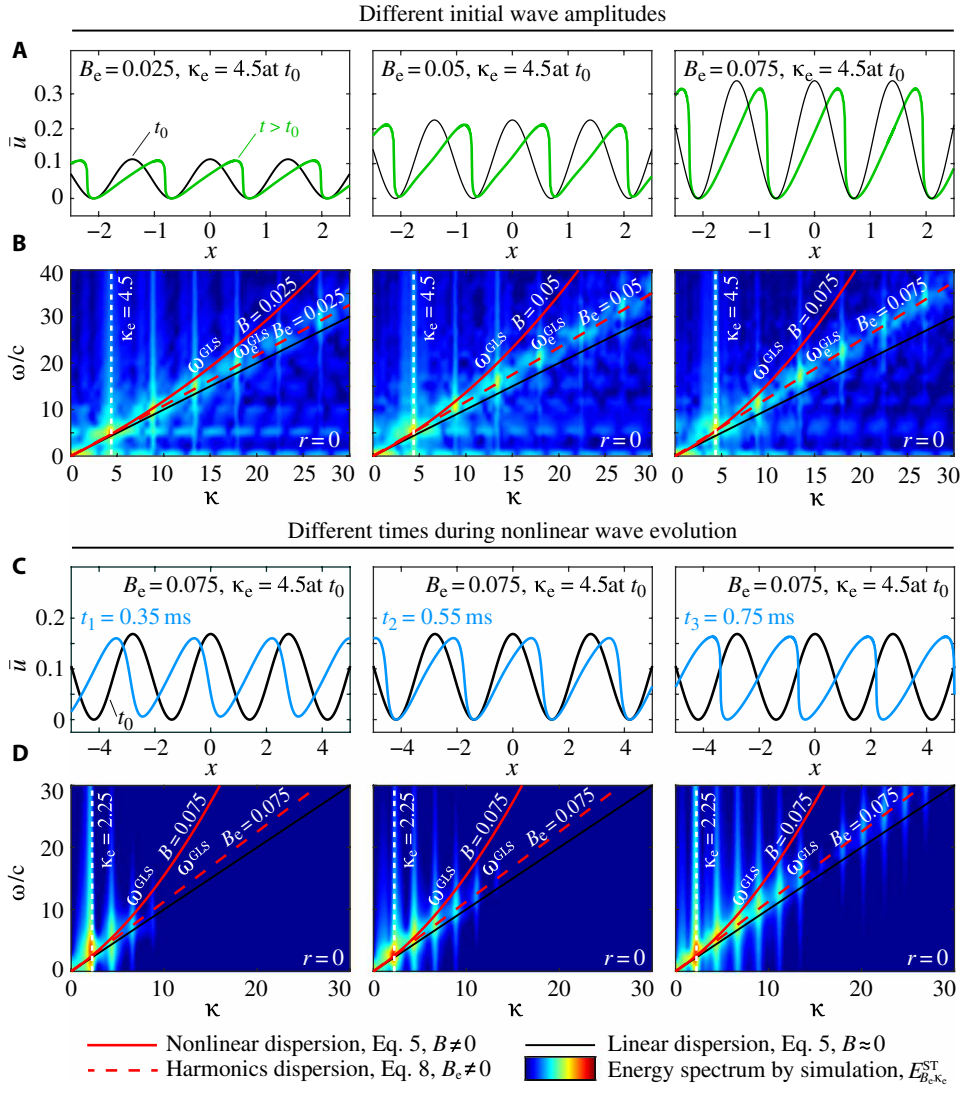

Fig. 2. Validation of theory for large wave amplitudes and at different times during wave evolution. Top two panels: Validation of the harmonics dispersion relation of Eq. 8 for nonlinear cosine waves of various prescribed amplitudes: $B_e = 0.025$, 0.05, and 0.075. (**A**) Spatial profile experiencing distortion (steepening) after some evolution in time. (**B**) Corresponding frequency–wave number spectra of harmonics. All results are based on the GLS measure. Bottom two panels: Validation of the harmonics dispersion relation of Eq. 8 for a nonlinear cosine wave at different stages of evolution, considering the following times during the simulation: $t_1 = 0.35$ ms, $t_2 = 0.55$ ms, and $t_3 = 0.75$ ms. (**C**) Spatial profile experiencing progressive distortion (steepening). (**D**) Corresponding frequency–wave number spectra of harmonics. All results are based on the GLS measure.

space on the wave profile at the time of excitation t_0 and at the two time instants t_1 and t_2 elucidates the nature of the temporal evolution of the wave number spectrum. At t_0, only a single harmonic exists (which is of the cosine excitation signal). As the wave evolves, the nonlinear effects increasingly cause distortion and generation of more energized higher harmonics, as shown in Fig. 3B. It is noticeable, however, that the wave number distribution of the harmonics gets established early in the simulation and is sustained as the evolution progresses. To investigate this aspect of harmonic generation further, we consider, in Fig. 2 (C and D), the same problem but for a slightly smaller excitation amplitude, $B_e = 0.075$. Figure 2C displays the spatial distortion at three different time instants, $t_1 = 0.35$ ms, $t_2 = 0.55$ ms, and $t_3 = 0.75$ ms. The corresponding spectral response is shown in Fig. 2D. Once again, the distribution is shown to get established at an early stage and sustain itself throughout the evolution; now, we see this to be the case in the frequency–wave number domain representing a state of spatiotemporal spectral invariance. These results confirm that the harmonics dispersion relation of Eq. 8 is applicable at all times during the nonlinear evolution as long as the wave remains stable.

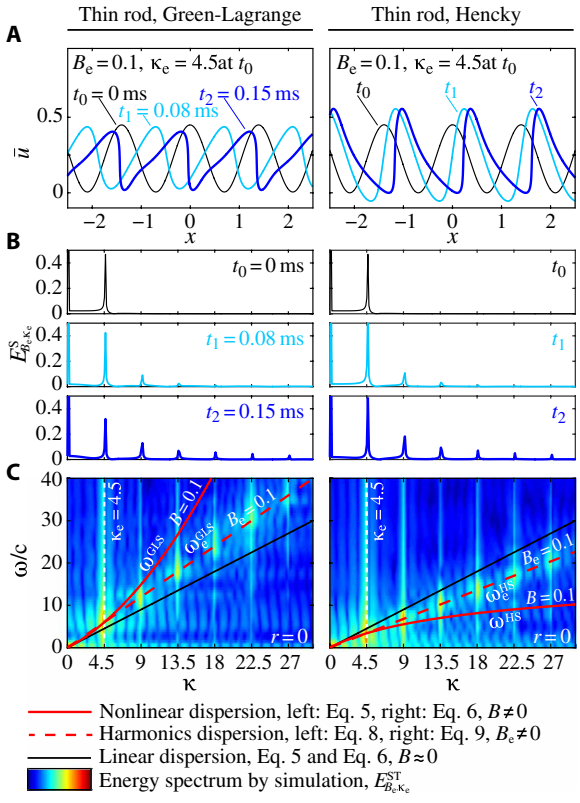

Fig. 3. Validation of theory for different types of nonlinearity. Strongly nonlinear cosine wave experiencing progressive distortion (steepening) and harmonic generation, considering both the GLS and HS models: (**A**) spatial profiles captured at three different times, (**B**) corresponding wave number spectra, and (**C**) frequency–wave number spectrum of harmonics at a highly evolved state demonstrating precise prediction by the harmonics dispersion relations of Eqs. 8 and 9, respectively. The spike at zero frequency in (B) is an artifact of the numerical Fourier transform.

Validation for linearly dispersive models

We also consider a thick rod under the GLS measure and propagate the same cosine excitation but now characterized by $B_e = 0.05$ and $\kappa_e = 4.5$ with various rod thicknesses. Unlike conventional techniques such as the method of characteristics that fall short in the presence of linear dispersion (*52*), our theory predicts the harmonic generation frequency–wave number spectrum even for systems that are linearly dispersive (e.g., $r \neq 0$), as is shown in Fig. 4. We observe that for all $r \neq 0$ cases (Fig. 4, C to E), the harmonics dispersion relation exhibits dispersion, indicating a nonlinear softening trend for the generated harmonics in line with the dispersive nature stemming from lateral inertia.

Validation for different initial wave profiles

Next, we simulate the nonlinear wave propagation of a localized pulse defined by a hyperbolic secant function, $\bar{f}(x,t) = B_e \kappa_e \mathrm{sech}(\kappa_e(x - ct))$. We apply $\bar{u}(x,t) = B_e\kappa_e[1 + \mathrm{sech}(\kappa_e(x - ct))]/2$, which is consistent with Eqs. 4 and 7, as the initial waveform at $t = 0$. Figure 5A shows the results for $B_e = 0.025$ and $\kappa_e = 6$. The initial wave packet propagates along the positive direction; also observed is a characteristic trailing wave of modest amplitude radiating in the opposite direction of the traveling wave. The spatial profile of the waves feature the eventual formation of shocks at the leading and trailing edges of the wave packet for the GLS and HS measures, respectively, in analogy with the behavior observed in Fig. 3A and analyzed further in the Supplementary Materials and fig. S1. In Fig. 5B, we consider excitations at two more κ_e values and superpose the Fourier-transformed

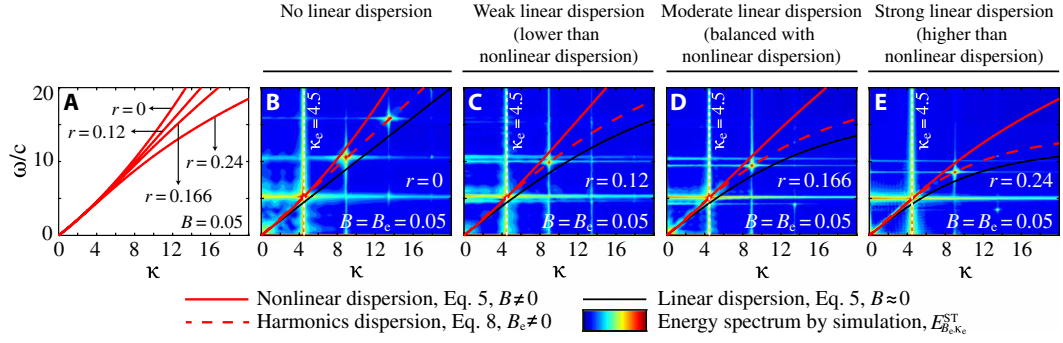

Fig. 4. Validation of theory for linearly dispersive models. Harmonics dispersion relation predicts harmonics generated by direct simulations for both linearly nondispersive ($r = 0$) and linearly dispersive ($r \neq 0$) rods: (**A**) effect of lateral inertia on the general NDR and (**B** to **E**) frequency–wave number spectra of harmonics with general NDR and harmonics dispersion relation for each case overlaid. Near balance of linear and nonlinear dispersion is demonstrated in (D). All results are based on the GLS measure, and a cosine wave is prescribed as an initial condition in the simulations.

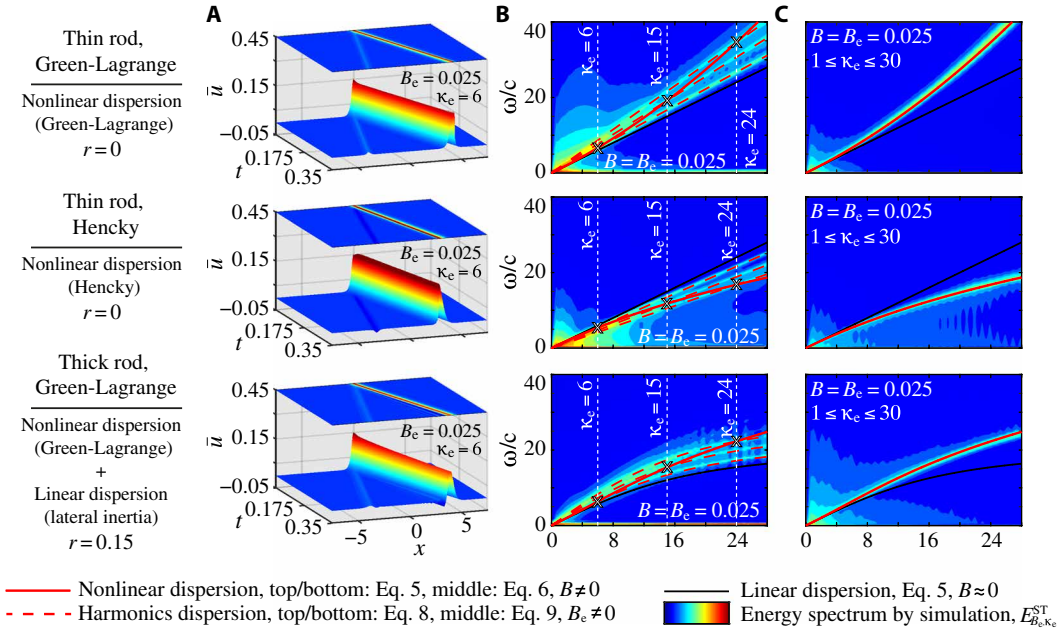

Fig. 5. Validation of theory for localized nonlinear waves and demonstration of the connection between harmonics dispersion relation and general NDR. (**A**) Space-time numerical simulation of a large-amplitude hyperbolic secant wave profile. (**B**) Frequency–wave number spectra showing distribution of harmonics in evolved field. The intersections of the harmonics dispersion relations (dashed red curves) for three distinct excitation wave numbers are shown to coincide with the general NDR for the selected value of wave amplitude. (**C**) Superposition of harmonics spectra from 30 distinct simulations covering a range of excitation wave numbers is shown to match with full conformity with the general NDR for the selected value of wave amplitude. Different cases are considered in each of the top, middle, and bottom panels.

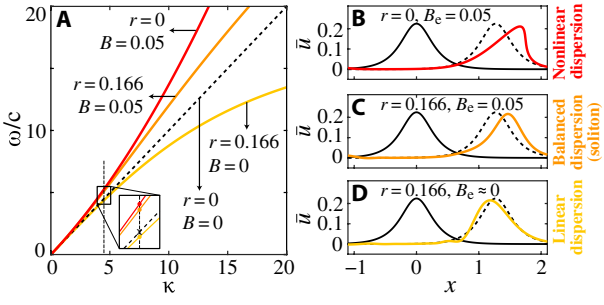

Fig. 6. Illustration of soliton synthesis in a thick rod. (**A**) Balance of hardening (nonlinear) dispersion with softening (linear) dispersion. The solid black curves represent an initial hyperbolic secant wave; the corresponding colored curves represent the evolved wave profile for (**B**) nonlinear dispersion, (**C**) nearly balanced dispersion (soliton), and (**D**) linear dispersion.

spectra for all three cases. It is seen that the analytical harmonics dispersion curves predict with full conformity the distribution of the harmonics for each of the excitations, including in the linearly dispersive case shown in the bottom panel. Note that since the hyperbolic secant function has a rich frequency content, the excited energy spectrum for each of the three cases displayed in Fig. 5B conforms continuously to the harmonics dispersion relations plotted in dashed red; this is in contrast to the cosine wave profile cases where the spectrum comprises discrete energy spots. Furthermore, the set of the intersections of each harmonics dispersion curve with its corresponding κ_e value exactly follows the path of the general NDR plotted in solid red. We learn from this perfect matching of intersections that the general NDR curve traces the fundamental harmonic associated with each excitation wave number (for a given value of B_e). This characteristic is confirmed further in Fig. 5C by superimposing the energy spectra of 30 separate simulations for distinct initial wave packets sharing the same amplitude $B_e = 0.025$ but covering the range of excitation wave numbers $\kappa_e = 1$ to 30, with increments of 1. Here, the quantity plotted is $\sum_{\kappa_e} E^{ST}_{B_e,\kappa_e} = \sum_{\kappa_e} [\ln | \mathcal{E}^{ST}_{B_e,\kappa_e} |]$, shown as a superposition of windows of energy spectra around the fundamental harmonic where each corresponds to a particular value of κ_e. The correlation of an NDR with a superposition of the fundamental harmonic frequencies discretely identified from the Fourier spectra corresponding to multiple wave number excitations, from separate simulations, was demonstrated in (*53*).

The results of Fig. 5 (B and C) confirm that our derived NDR and harmonics dispersion relation hold for arbitrary excitation profiles such as the hyperbolic secant function considered, as long as the excitation signal is initially characterized by B_e and κ_e and is consistent with Eqs. 4 and 7. Two more examples of different initial wave profiles, namely, a Gaussian profile and a Lorentzian profile, are examined in the Supplementary Materials and are shown to be also accurately characterized by the NDR and harmonics dispersion relation.

Soliton synthesis by general NDR

Solitons research traces back to its first observation in a canal by J. S. Russell (*54*) and key early theoretical developments that followed (*55*, *56*). Other than their solitary spatial profile, a unique aspect of this class of waves is their inherent stability which is commonly attributed to a balance between nonlinear and dispersion effects (*52*). Using the general NDR, we are able to find a condition for

balance between hardening dispersion (stemming from the nonlinear kinematics) and softening dispersion (stemming from the linear lateral inertia). This represents a formal approach for the analysis, characterization, and engineering of solitons. This approach has been presented recently by the authors in the context of 1D periodic rods (*57*). For a thick rod, we formulate the soliton synthesis condition as

$$r = \arg\min\{\|\omega_{GLS}/c - \alpha B\kappa\|_{[0,1]}/\max_{[0,1]}(\omega_{GLS}/c) \leq 1\%, \alpha \in \mathbb{R}\} \quad (10)$$

which gives an optimal value of $r = 0.166$ for $B = 0.05$. These values generate a linear-nonlinear dispersion balance within 1% error for the range $0 \leq B\kappa \leq 1$, which is the case displayed in Fig. 4D, where the general NDR appears nearly as a perfect linear (straight) curve. The harmonic generation of this nearly balanced wave is dispersive. Thus, while minimum dispersion in the general NDR is needed for the creation of a soliton (with some error tolerance for a given $B\kappa$ range), the associated harmonic generation spectrum is not necessarily nondispersive. Figure 6A decomposes the balancing components in the general NDR, and Fig. 6 (B to D) illustrates the effect in the spatial domain showing, in Fig. 6C, the stable and nearly invariant propagation of a synthesized soliton. Future work may extend this soliton synthesis concept to more complex models, for example, rods/beams with varying cross section (*58*, *59*) or prestretch (*60*), to name a few.

DISCUSSION

We have provided a unified theory of nonlinear waves consisting of a general NDR and a harmonics dispersion relation, where the former encompasses the latter. A general NDR defines, (i) for a given amplitude B and wave number κ, the instantaneous dispersion of a nonlinear wave (*8*) and, (ii) for a given excitation amplitude B_e, the frequency–wave number trajectory of the fundamental harmonic in a superposition of isolated windows of Fourier-transformed nonlinear wave fields spanning a range of excitation wave numbers κ_e. Prescription of a condition for soliton synthesis is a natural outcome of the general NDR, as demonstrated in Figs. 4 (A and D) and 6 (A and C). A harmonics dispersion relation, which is a novel concept, defines the frequency–wave number spectrum of the generated harmonics in a nonlinear wave field for a given excitation amplitude B_e and wave number κ_e. This relation effectively unravels the inner makings of a nonlinear wave. It is derived directly from the governing nonlinear PDE; thus, it provides a pathway for prediction of the spectral content of harmonic generation without knowledge of the time-dependent spatial solution or any treatment of the problem in the spatial-temporal domain. The HDR is shown to be a special case of the general NDR by comparing Eqs. 8 and 9 to 5 and 6. This connection establishes a fundamental unification of two key tenets of wave propagation: nonlinear dispersion and harmonic generation. Both relations are derived exactly (i.e., without any expansions or perturbation analysis).

As shown in the diverse sets of examples given, considering thin and thick elastic rods, there is no limitation by the type and strength of the nonlinearity, or by the shape of the initial wave profile provided that it belongs to the family of functions $\mathcal{F}$. There is also no restriction on the presence of linear dispersion. The derived relations are applicable at any state of evolution in time as long as the wave is balanced or has not yet reached its breaking point if unbalanced. These findings underscore the nature of general nonlinear dispersion and harmonic generation dispersion as time-independent characteristics of the medium and its wave propagation properties, for a given amplitude and a given class of initial profiles for the evolving or balanced waveform.

Given that the theory at its foundation is based on the introduction of the traveling wave conditions of Eqs. 4 and 7, it is, in principle, agnostic to the type of wave considered. It is therefore applicable to other disciplines of wave propagation beyond elastic waves, as well as being amenable to extension to multidimensional problems.

MATERIALS AND METHODS

The numerical results presented in this study were obtained using an in-house code; see details in the Supplementary Materials. The material properties considered are for aluminum: $\rho = 2700$ kg/m^3, $E = 70$ GPa, and $\nu = 0.33$. All reported units are in the SI system.

SUPPLEMENTARY MATERIALS

Supplementary material for this article is available at https://science.org/doi/10.1126/sciadv.abl3695

REFERENCES AND NOTES

1. G. B. Whitham, *Linear and Nonlinear Waves* (John Wiley & Sons, 1974).
2. K. Nishijima, *Fields and Particles: Field Theory and Dispersion Relations* (W. A. Benjamin, 1969).
3. R. Carretero-González, D. J. Frantzeskakis, P. G. Kevrekidis, Nonlinear waves in Bose–Einstein condensates: Physical relevance and mathematical techniques. *Nonlinearity* **21**, R139–R202 (2008).
4. D. F. Parker, The nonlinear dispersion of Rayleigh waves. *Physica D* **16**, 385–397 (1985).
5. G. Chakraborty, A. K. Mallik, Dynamics of a weakly non-linear periodic chain. *Int. J. Nonlin. Mech.* **36**, 375–389 (2001).
6. P. Cobelli, P. Petitjeans, A. Maurel, V. Pagneux, N. Mordant, Space-time resolved wave turbulence in a vibrating plate. *Phys. Rev. Lett.* **103**, 204301 (2009).
7. R. K. Narisetti, M. Ruzzene, M. J. Leamy, A perturbation approach for predicting wave propagation in one-dimensional nonlinear periodic structures. *J. Vib. Acoust.* **132**, 031001 (2010).
8. M. H. Abedinnasab, M. I. Hussein, Wave dispersion under finite deformation. *Wave Motion* **50**, 374–388 (2013).
9. W. Lee, G. Kovačič, D. Cai, Generation of dispersion in nondispersive nonlinear waves in thermal equilibrium. *Proc. Natl. Acad. Sci. U.S.A.* **110**, 3237–3241 (2013).
10. P. K. Shukla, I. Kourakis, B. Eliasson, M. Marklund, L. Stenflo, Instability and evolution of nonlinearly interacting water waves. *Phys. Rev. Lett.* **97**, 094501 (2006).
11. M. Onorato, A. R. Osborne, M. Serio, Modulational instability in crossing sea states: A possible mechanism for the formation of freak waves. *Phys. Rev. Lett.* **96**, 014503 (2006).
12. P. Clark di Leoni, P. J. Cobelli, P. D. Mininni, Wave turbulence in shallow water models. *Phys. Rev. E* **89**, 063025 (2014).
13. E. Herbert, N. Mordant, E. Falcon, Observation of the nonlinear dispersion relation and spatial statistics of wave turbulence on the surface of a fluid. *Phys. Rev. Lett.* **105**, 144502 (2010).
14. V. E. Gusev, W. Lauriks, J. Thoen, Dispersion of nonlinearity, nonlinear dispersion, and absorption of sound in microinhomogeneous materials. *J. Acoust. Soc. Am.* **103**, 3216–3226 (1998).
15. I. V. Shadrivov, A. A. Sukhorukov, Y. S. Kivshar, A. A. Zharov, A. D. Boardman, P. Egan, Nonlinear surface waves in left-handed materials. *Phys. Rev. E* **69**, 016617 (2004).
16. I. Kourakis, P. K. Shukla, Nonlinear propagation of electromagnetic waves in negative-refraction-index composite materials. *Phys. Rev. E* **72**, 016626 (2005).
17. P. H. Yoon, R. Gaelzer, T. Umeda, Y. Omura, H. Matsumoto, Harmonic Langmuir waves. I. Nonlinear dispersion relation. *Phys. Plasmas* **10**, 364–372 (2003).
18. J. H. Huang, R. Chang, P. T. Leung, D. P. Tsai, Nonlinear dispersion relation for surface plasmon at a metal–kerr medium interface. *Opt. Commun.* **282**, 1412–1415 (2009).
19. P. Ginzburg, A. Hayat, N. Berkovitch, M. Orenstein, Nonlocal ponderomotive nonlinearity in plasmonics. *Opt. Lett.* **35**, 1551–1553 (2010).
20. R. Hager, K. Hallatschek, Nonlinear dispersion relation of geodesic acoustic modes. *Phys. Rev. Lett.* **108**, 035004 (2012).
21. D. C. Fritts, M. J. Alexander, Gravity wave dynamics and effects in the middle atmosphere. *Rev. Geophys.* **41**, 1003 (2003).

22. L. Debnath, On linear and nonlinear Rossby waves in an ocean. *J. Math. Anal. Appl.* **333**, 164–190 (2007).
23. J. P. Boyd, Nonlinear equatorial waves, in *Dynamics of the Equatorial Ocean*, J. Boyd, Ed. (Springer, 2018), pp. 329–404.
24. M. Forsberg, G. Brodin, Harmonic generation of gravitational wave induced Alfvén waves. *Phys. Rev. D* **77**, 024050 (2008).
25. A. S. Davydov, The theory of contraction of proteins under their excitation. *J. Theor. Biol.* **38**, 559–569 (2018).
26. A. Mvogo, G. H. Ben-Bolie, T. C. Kofané, Solitary waves of α-helix propagation in media with arbitrary inhomogeneities. *Eur. Phys. J. B.* **86**, 217 (2013).
27. C. S. Gardner, J. M. Greene, M. D. Kruskal, R. M. Miura, Method for solving the Korteweg-deVries equation. *Phys. Rev. Lett.* **19**, 1095–1097 (1967).
28. P. D. Lax, Integrals of nonlinear equations of evolution and solitary waves. *Commun. Pur. Appl. Math.* **21**, 467–490 (1968).
29. V. E. Zakharov, L. D. Faddeev, Korteweg-de vries equation: A completely integrable Hamiltonian system. *Funct. Anal. Appl.* **5**, 280–287 (1971).
30. M. J. Ablowitz, D. J. Kaup, A. C. Newell, H. Segur, The inverse scattering transform-fourier analysis for nonlinear problems. *Stud. Appl. Math.* **53**, 249–315 (1974).
31. G. B. Whitham, Non-linear dispersive waves. *Proc. R. Soc. A* **283**, 238–261 (1965).
32. H. W. Schürmann, V. S. Serov, Y. V. Shestopalov, TE-polarized waves guided by a lossless nonlinear three-layer structure. *Phys. Rev. E* **58**, 1040–1050 (1998).
33. P. A. Franken, A. E. Hill, C. W. Peters, G. Weinreich, Generation of optical harmonics. *Phys. Rev. Lett.* **7**, 118–119 (1961).
34. M. A. Breazeale, D. O. Thompson, Finite-amplitude ultrasonic waves in aluminum. *Appl. Phys. Lett.* **3**, 77–78 (1963).
35. A. Hikata, B. B. Chick, C. Elbaum, Effect of dislocations on finite amplitude ultrasonic waves in aluminum. *Appl. Phys. Lett.* **3**, 195–197 (1963).
36. A. A. Gedroitz, V. A. Krasilnikov, Elastic waves of finite amplitude and deviations from Hooke's law. *Sov. Phys. JETP* **16**, 1122–1131 (1963).
37. A. V. Buryak, Y. S. Kivshar, Solitons due to second harmonic generation. *Phys. Lett. A* **197**, 407–412 (1995).
38. K. Hasselmann, On the non-linear energy transfer in a gravity-wave spectrum, Part 1. General theory. *J. Fluid Mech.* **12**, 481–500 (1962).
39. D. J. Benney, P. G. Saffman, Nonlinear interaction of random waves in a dispersive medium. *Proc. R. Soc. A* **289**, 301–320 (1966).
40. R. N. Thurston, M. J. Shapiro, Interpretation of ultrasonic experiments on finite-amplitude waves. *J. Acoust. Soc. Am.* **41**, 1112–1125 (1967).
41. H. F. Tiersten, J. C. Baumhauer, Second harmonic generation and parametric excitation of surface waves in elastic and piezoelectric solids. *J. Appl. Phys.* **45**, 4272–4287 (1974).
42. R. B. Thompson, H. F. Tiersten, Harmonic generation of longitudinal elastic waves. *J. Acoust. Soc. Am.* **62**, 33–37 (1977).
43. B. A. Auld, *Acoustic Fields and Waves in Solids, Vols. I and II* (Wiley, 1973).
44. M. Deng, Cumulative second-harmonic generation of lamb-mode propagation in a solid plate. *J. Appl. Phys.* **85**, 3051–3058 (1999).
45. W. J. N. de Lima, M. F. Hamilton, Finite-amplitude waves in isotropic elastic plates. *J. Sound Vib.* **265**, 819–839 (2003).
46. A. Hikata, B. B. Chick, C. Elbaum, Dislocation contribution to the second harmonic generation of ultrasonic waves. *J. Appl. Phys.* **36**, 229–236 (1965).
47. M. A. Breazeale, J. Ford, Ultrasonic studies of the nonlinear behavior of solids. *J. Appl. Phys.* **36**, 3486–3490 (1965).
48. K. H. Matlack, J. Y. Kim, L. J. Jacobs, J. Qu, Review of second harmonic generation measurement techniques for material state determination in metals. *J. Nondestruct. Eval.* **34**, 273 (2015).
49. M. H. Abedinnasab, M. V. Bastawrous, M. I. Hussein, Explicit dispersion relation for strongly nonlinear flexural waves using the homotopy analysis method. *Nonlinear Dynam.* **99**, 737–752 (2020).
50. B. R. Seth, Generalized strain measure with applications to physical problems, in *IUTAM Symposium on Second Order Effects in Elasticity, Plasticity and Fluid Mechanics* (Pergamon Press, 1962), pp. 1–14.
51. R. Hill, On constitutive inequalities for simple materials—I. *J. Mech. Phys. Solids* **16**, 229–242 (1968).
52. M. J. Ablowitz, *Nonlinear Dispersive Waves: Asymptotic Analysis and Solitons* (Cambridge Univ. Press, 2011).
53. R. Ganesh, S. Gonella, Spectro-spatial wave features as detectors and classifiers of nonlinearity in periodic chains. *Wave Motion* **50**, 821–835 (2013).
54. J. S. Russell, Report on waves, in *14th Meeting of the British Association for the Advancement of Science* (John Murray, London, 1844), pp. 311–390.
55. D. Korteweg, G. de Vries, XLI. On the change of form of long waves advancing in a rectangular canal, and on a new type of long stationary waves. *Philos. Mag.* **39**, 422–443 (1895).
56. J. H. Adlam, J. E. Allen, The structure of strong collision-free hydromagnetic waves. *Philos. Mag.* **3**, 448–455 (1958).
57. M. I. Hussein, R. Khajehtourian, Nonlinear Bloch waves and balance between hardening and softening dispersion. *Proc. R. Soc. A* **474**, 20180173 (2018).
58. A. M. Samsonov, G. V. Dreiden, A. V. Porubov, I. V. Semenova, Longitudinal-strain soliton focusing in a narrowing nonlinearly elastic rod. *Phys. Rev. B* **57**, 5778–5787 (1998).
59. L. Liu, M. I. Hussein, Wave motion in periodic flexural beams and characterization of the transition between Bragg scattering and local resonance. *J. Appl. Mech.* **79**, (2012).
60. F. Garbuzov, K. R. Khusnutdinova, I. V. Semenova, On Boussinesq-type models for long longitudinal waves in elastic rods. *Wave Motion* **88**, 129–143 (2019).
61. M. C. Remillieux, R. A. Guyer, C. Payan, T. J. Ulrich, Decoupling nonclassical nonlinear behavior of elastic wave types. *Phys. Rev. Lett.* **116**, 115501 (2016).
62. H. H. Dai, Y. Huo, Solitary shock waves and other travelling waves in a general compressible hyperelastic rod. *Proc. R. Soc. A* **456**, 331–363 (2000).
63. D. H. Johnson, D. E. Dudgeon, *Array Signal Processing: Concepts and Techniques* (Simon & Schuster, 1992).

Acknowledgments: We express utmost gratitude to M. J. Ablowitz for sharing experience and insights and for helping us see where our work sits within the full scope of nonlinear wave science. We are also thankful to M. A. Hoefer and C. A. Felippa for fruitful discussions and to graduate students M. V. Bastawrous and M. M. Khanegahi for assistance in checking and reproducing the results. **Funding:** This work was partially supported by the NSF CAREER Grant no. 1254937. **Author contributions:** R.K. and M.I.H. designed and performed research, analyzed the results, and wrote the paper. **Competing interests:** The authors declare that they have no competing interests. **Data and materials availability:** All data are generated directly using the equations presented here and the accompanying Supplementary Materials.

Submitted 9 July 2021
Accepted 19 October 2021
Published 8 December 2021
10.1126/sciadv.abl3695

Time-independent harmonics dispersion relation for time-evolving nonlinear waves

Romik KhajehtourianMahmoud I. Hussein

Sci. Adv., 7 (50), eabl3695.

Science Advances
AAAS

Supplementary Materials for

Time-independent harmonics dispersion relation for time-evolving nonlinear waves

Romik Khajehtourian and Mahmoud I. Hussein

*Corresponding author. Email: mih@colorado.edu

Published 8 December 2021, *Sci. Adv.* **7**, eabl3695 (2021)
DOI: 10.1126/sciadv.abl3695

The PDF file includes:

Supplementary Text
Figs. S1 to S3
Table S1
Legends for movies S1 and S2
References

Other Supplementary Material for this manuscript includes the following:

Movies S1 and S2

Wave steepening and stability analysis

To investigate the nonlinear wave distortion and breaking phenomena, we consider the limiting configuration of a thin rod where the lateral inertia is ignored by setting $r = 0$.* In this medium, a traveling wave profile with finite-amplitude B will experience in the course of its evolution forward self-steepening in the case of Green-Lagrange nonlinearity and backward self-steepening in the case of Hencky nonlinearity. In forward steepening, the leading edge has a steeper slope than the trailing edge; and vice versa in backward steepening. Thus Green-Lagrange-induced steepening takes place in the direction of propagation and represents a *dispersion hardening* effect (57) that eventually leads to the formation of a shock $\partial_x \bar{u} = -\infty$. In contrast, Hencky-induced steepening causes a tilt opposite to the direction of propagation and represents a *dispersion softening* effect (61) that eventually leads to the formation of a shock $\partial_x \bar{u} = \infty$. Both scenarios are demonstrated in Fig. S1. Consider $m(x,t) < 0$ and $M(x,t) > 0$ to be the minimum and maximum value of $\partial_x \bar{u}$ as a function of time. There exist a finite shock time τ_{S} when at least one point of the wave profile slope becomes vertical, $m \to -\infty$ and $M \to \infty$, and a shock forms at the leading edge in the GLS case and at the trailing edge in the HS case (62). At $t = \tau_{\mathrm{S}}$, the nonlinear wave becomes unstable. These effects are quantified by characteristic lines, as demonstrated in the inset of Fig. S1.

The stability of this nonlinear thin rod can be locally evaluated using eigenvalues of Eq. (S1) which is the equivalent first-order system of Eq. (2) ignoring the effects of lateral inertia,

$$\begin{aligned} \partial_\xi \bar{U} &= \bar{V}, \\ \partial_\xi \bar{V} &= \frac{\kappa^2}{\omega^2} \partial_{\xi\xi} (\alpha \bar{U} + \beta \mathcal{N}(\bar{U})). \end{aligned} \tag{S1}$$

By analyzing this system, we find two distinct real eigenvalues, one negative and one positive, which collide into each other on $\bar{V} = 0$. The positive eigenvalue indicates that the system is unstable and the solutions are in the form of breaking waves.

The position and time of the onset of shock may be determined by solving $\partial_{\bar{u}} x(\bar{u}) = 0$ (equivalent to $|\partial_x \bar{u}(x)| = \infty$) for a known solution, and setting $\partial_{\bar{u}\bar{u}} x(\bar{u}) = 0$ as a necessary condition to ensure the uniqueness of $\bar{u}(x)$.

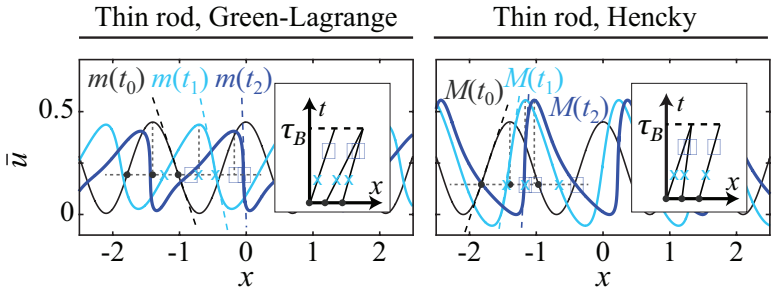

Fig. S1. | **Cosine wave experiencing distortion and harmonic generation.** Spatial profiles captured at $t_0 = 0$ ms, $t_1 = 0.08$ ms, and $t_2 = 0.15$ ms are shown. Initial amplitude is $B_{\mathrm{e}} = 0.1$ and initial wavenumber is $\kappa_{\mathrm{e}} = 4.5$. Inset shows the corresponding characteristic lines. Results are for a GLS case (left) and an HS case (right).

*Throughout the Supplementary Materials document, we use the same material properties considered in the main article.

Generic form for general NDR and harmonics dispersion relation

The general NDR may be expressed directly in terms of the nonlinear function, $\mathcal{N}(\bar{U})$, and the strain-gradient at $\xi = 0$, $\bar{U}(0)$, as

$$\omega = \frac{c\kappa}{\sqrt{1+\gamma\kappa^2}}\sqrt{1+\frac{\mathcal{N}[\bar{U}(0)]}{\bar{U}(0)}}, \tag{S2}$$

where $\mathcal{N}(\bar{U}) = 3\bar{U}^2/2 + \bar{U}^3/2$ for the GLS measure, and $\mathcal{N}(\bar{U}) = \ln(1+\bar{U})/(1+\bar{U})$ for the HS measure and $\bar{U}(0) = B\kappa$. Equation (S2) yields Eqs. (5) and (6).

Similarly, the harmonics dispersion relation may be expressed directly in terms of the nonlinear function, $\mathcal{N}(\bar{U}_\mathrm{e})$, and the strain-gradient at $\xi = 0$, $\bar{U}_\mathrm{e}(0)$, as

$$\omega = \frac{c\kappa}{\sqrt{1+\gamma\kappa^2}}\sqrt{1+\frac{\mathcal{N}[\bar{U}_\mathrm{e}(0)]}{\bar{U}_\mathrm{e}(0)}}, \tag{S3}$$

where $\bar{U}_\mathrm{e}(0) = B_\mathrm{e}\kappa_\mathrm{e}$. Equation (S3) yields Eqs. (8) and (9).

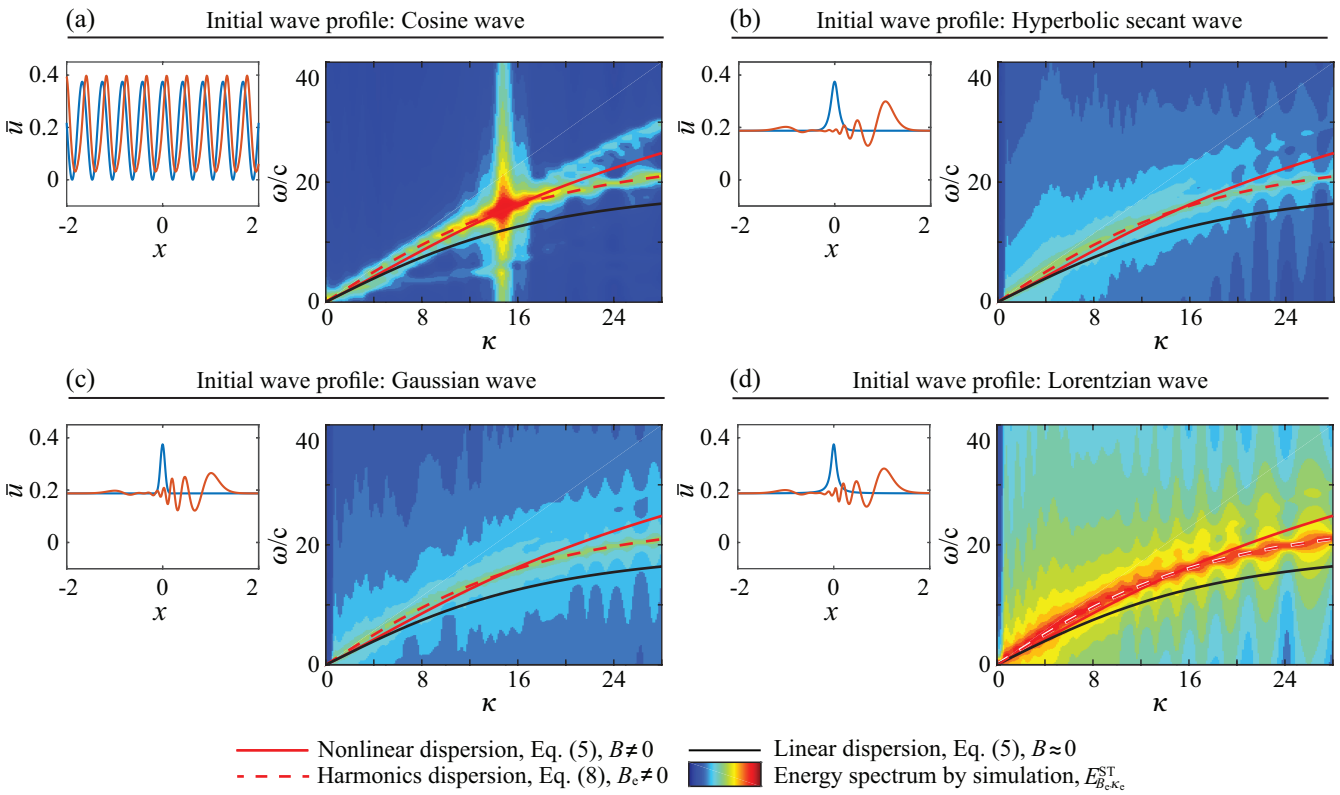

Fig. S2. | **Validation of theory for different types of initial wave profiles**. Demonstration of validity of the harmonic dispersion relation [Eq. (8) for GLS nonlinearity] in capturing the nonlinear harmonics frequency-wavenumber spectrum for four different types of initial signals: (a) cosine, (b) hyperbolic secant, (c) Gaussian, and (d) Lorentzian. The wave amplitude for all general NDR curves (solid red lines) is $B = 0.025$; and the excitation wave amplitude and excitation wavenumber for all harmonic dispersion relation curves (dashed red lines) and numerical simulation results are $B_\mathrm{e} = 0.025$ and $\kappa_\mathrm{e} = 15$, respectively. All results here are for $r = 0.15$, which is the same value of the polar radius of gyration selected for the results presented in the third row of Fig. 5 in the main article. Clearly, the prediction of our derived harmonic dispersion relation matches perfectly with the space-time Fourier spectrum from the numerical simulations for all four types of initial signals. Also shown at the top left of each sub-figure is the spatial profile of the signal initially (blue) and at a later stage after its nonlinear evolution (orange).

Validation of harmonic dispersion relation for different initial wave profiles: Additional Examples

The applicability of the harmonics dispersion relation concept in capturing the harmonics for different forms of an initial signal/waveform has been demonstrated in the main article for a cosine signal and a hyperbolic secant signal. In this section, we consider these two initial signal forms again (for a different combination of B_e and κ_e to avoid repetition) and add two more examples of initial signals, namely, a Gaussian initial signal and a Lorentzian initial signal. These four signal types are considered in the presence of linear dispersion in the form of lateral inertia (i.e., with $\gamma \neq 0$) in order to add further complexity and generality. As shown in Fig. S2, the theory [Eqs. (8) in the main article] provides a perfect prediction of the harmonics distribution within the frequency-wavenumber spectrum. The parameters selected for these examples are given in Table S1.

Table S1. | Parameters used for different initial signal examples presented in Fig. S2

Parameter	γ	r	B_e	κ_e
Value	0.0025	0.15	0.025	15

Computational approach: Description and verification

Description—We simulate the wave propagation governed by Eq. (1) using a spectral method for the spatial variable in conjunction with an efficient explicit time-stepping method. The nonlinear PDEs are discretized with the discrete Fourier transform (DFT) in space and marched in time using a numerical integration scheme. We consider $\bar{u}_j$ as a discrete function on an N-point spatial grid x_j, $j = 1, \ldots, N$. The DFT is defined by $\widehat{u}_k = h \sum_j \mathrm{e}^{-\mathrm{i}kx_j} \bar{u}_j$, for $k = -N/2 + 1, ..., N/2$, and the inverse discrete Fourier transform (IDFT) by $\bar{u}_j = \frac{1}{2\pi} \sum_k \mathrm{e}^{\mathrm{i}kx_j} \widehat{u}_k$, for each point. Here, $x_j = jh$ where $h = 2\pi/N$ is the spacing of the grid points, and k is the Fourier wavenumbers. We apply $\partial_t \bar{u} = \bar{v}$ followed by the DFT on Eq. (1) to form the corresponding first-order system

$$\partial_t \begin{bmatrix} \widehat{u} \\ \widehat{v} \end{bmatrix} = \begin{bmatrix} 0 & 0 \\ -\frac{\alpha k^2}{1+\gamma k^2} & 0 \end{bmatrix} \begin{bmatrix} \widehat{u} \\ \widehat{v} \end{bmatrix} + \begin{bmatrix} \widehat{v} \\ -\frac{\beta k^2}{1+\gamma k^2} \mathcal{F}_\mathcal{T}(\mathcal{N}) \end{bmatrix}, \tag{S4}$$

where $\mathcal{F}_\mathcal{T}(.)$ denotes the Fourier transform of the considered function. Differentiating the transformation $[\widehat{\mathsf{u}}, \widehat{\mathsf{v}}]^\mathrm{T} = \mathbf{\Gamma} [\widehat{u}, \widehat{v}]^\mathrm{T}$ with respect to time, with $\mathbf{\Gamma} = [I, 0; \alpha k^2 \Delta t/(1+\gamma k^2), I]$ being the integral factor of Eq. (S4), followed by the substitution of the $\partial_t \widehat{u}$ and $\partial_t \widehat{v}$ values from Eq. (S4) and $\widehat{u}$ and $\widehat{v}$ from the inverse transformation $[\widehat{u}, \widehat{v}]^\mathrm{T} = \mathbf{\Gamma}^{-1} [\widehat{\mathsf{u}}, \widehat{\mathsf{v}}]^\mathrm{T}$, produces the following numerically integrable system (returning to continuous notation for convenience):

$$\begin{aligned} \partial_t \widehat{\mathsf{u}} &= -\frac{\alpha k^2 \Delta t}{1+\gamma k^2} \widehat{\mathsf{u}} + \widehat{\mathsf{v}}, \\ \partial_t \widehat{\mathsf{v}} &= \frac{\alpha k^2 \Delta t}{1+\gamma k^2} \left(-\frac{\alpha k^2 \Delta t}{1+\gamma k^2} \widehat{\mathsf{u}} + \widehat{\mathsf{v}}\right) - \frac{\beta k^2}{1+\gamma k^2} \mathcal{F}(\mathcal{N}). \end{aligned} \tag{S5}$$

We use the fourth-order explicit Runge-Kutta time-stepping scheme to integrate Eq. (S5). Then the inverse transformation is applied followed by IDFT on $[\widehat{\mathsf{u}}, \widehat{\mathsf{v}}]^\mathrm{T}$ to obtain $\bar{u}(x,t)$. The direction of wave propagation in the simulation is dictated by the initial velocity condition we prescribe. Now that we have the space-time solution, we apply Fourier analysis to the spatio-temporal wave-field discrete

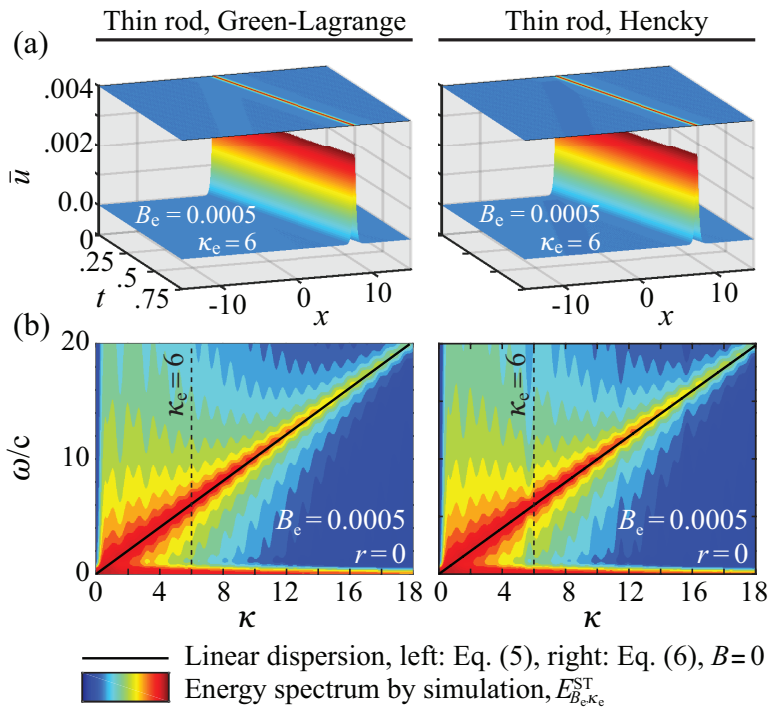

Fig. S3. | **Verification of computational approach on a linear nondispersive rod (GLS measure in left column and HS measure in right column)**. (a) Infinitesimal-strain space-time solution for $B_e = 0.0005$ and $\kappa_e = 6$. (b) A representation of the energy spectrum obtained by numerical Fourier transformation. Corresponding exact dispersion curves from Eqs. (4) and (5) are overlaid as solid lines. Time and space units are [ms] and [m], respectively.

data $\bar{u}_{p,q}, p = 0, 1, ..., N-1, q = 0, 1, ..., T-1$ to evaluate $\mathcal{E}^{\mathrm{ST}}_{l,n} = \frac{1}{NT}\sum_p \sum_q \mathrm{e}^{-2\pi \mathrm{i}(lp/N + nq/T)} \bar{u}_{p,q}$, for $l = 0, 1, ..., N$ and $n = 0, 1, ..., T$ defining T as the number of time steps. This yields the numerical frequency-wavenumber energy spectrum $\mathcal{E}^{\mathrm{ST}}(\kappa, \omega)$ (53,63).

Verification—For basic verification of the computational approach, we analyze a rod at the limits of $B \to 0, r \to 0$ to recover the linear dispersion relation $\omega = c\kappa$ from Eqs. (4) and (5). We set $r = 0$ and choose a small amplitude, $B = 0.0005$, instead of setting $B = 0$ to avoid numerical instabilities in the simulations. The excitation profile considered is the same as the one studied in Fig. 3. These parameters generate a practically linear nondispersive wave. The space-time solution is shown in Fig. S3a and the corresponding energy spectrum is plotted in Fig. S3b; we clearly see that numerical energy spectrum perfectly coincides with the infinitesimal-strain dispersion relation, thus confirming the verification.

Supplementary movie captions

Movie S1.

Animation (solid red) showing the evolution of a nonlinear wave based on a Green-Lagrange strain-measure, which represents a hardening nonlinearity. A forward self-steepening effect is observed as the wave propagates from left to right. This case has no dispersion in the linear (low-amplitude)limit. In the background, an animation (dashed black) of a corresponding linear wave is shown for comparison.

Movie S2.

Animation (solid brown) showing the evolution of a nonlinear wave based on a Hencky strain measure, which represents a softening nonlinearity. A backward self-steepening effect is observed as the wave propagates from left to right. This case has no dispersion in the linear (low-amplitude) limit. In the background, an animation (dashed black) of a corresponding linear wave is shown for comparison.